© Pol J Radiol 2022; 87: e678-e687
DOI: https://doi.org/10.5114/pjr.2022.123829

Received: 18.04.2022
Accepted: 08.08.2022
Published: 27.12.2022

Polish Journal of Radiology

http://www.polradiol.com

Original paper

Comparative study of true and virtual non-contrast imaging generated from dual-layer spectral CT in patients with upper aerodigestive tract cancer

Varalee Mingkwansook[A,C,D,E,F], Krittiya Puwametwongsa[B,C], Arvemas Watcharakorn[F], Thanapat Dechasasawat[D]

Thammasat University, Bangkok, Thailand

Abstract

Purpose: Dual-layer spectral computed tomography (DLSCT) is a novel CT platform of dual-energy CT. Virtual non-contrast (VNC) imaging theoretically resembles true non-contrast (TNC) imaging by subtracting iodine attenuation from post-contrast data. We aimed to compare qualitative and quantitative datasets between TNC and VNC in patients with upper aerodigestive tract cancer (UATC) and to evaluate the potential radiation dose reduction obtained by omitting the TNC phase.

Material and methods: The study included 61 patients with UATC who underwent DLSCT. The CT protocol included TNC and post-contrast phases. The VNC images were reconstructed from the post-contrast phase. The differences of mean CT attenuation values, imaging noise, and image quality for TNC and VNC images were compared. The effective radiation doses of a biphasic TNC and post-contrast CT protocol were compared with a single-phase protocol (post-contrast CT with VNC reconstruction).

Results: There were a total of 732 ROIs from TNC and VNC. There was no statistical difference in the mean CT attenuation values between TNC and VNC images for all tissue types (p = 0.09-0.44), except for the buccal fat pad. Overall, 85.3% of cases revealed a difference of less than 10 HU. There was no significant difference in mean imaging noise (p = 0.5455) and image quality (p = 0.3214) between 2 acquisitions. All VNC images had acceptable quality for diagnostic purposes. The potential dose reduction by omitting the TNC was 49.5 ± 3.5%.

Conclusion: VNC could replace TNC images in patients with UATC, with good image quality and the advantage of radiation dose reduction.

Key words: dual-layer spectral computed tomography (DLSCT), dual-energy computed tomography, virtual non-contrast (VNC), true non-contrast (TNC), upper aerodigestive tract cancer (UATC).

Introduction

Dual-layer spectral computed tomography (DLSCT) is a novel computed (CT) platform of dual-energy computed tomography (DECT) in which 2 sets of attenuating data are acquired from specialized layered detectors. This new technique enhanced diagnostic performance in head and neck cancer as compared to conventional single-energy computed tomography (SECT) [1-6]. Virtual non-contrast (VNC) imaging is one of the promising applications of DLSCT which subtract iodine attenuation from post-contrast data and generate imaging theoretically resembling true non-contrast (TNC) imaging [1-6].

Correspondence address:
Varalee Mingkwansook, Thammasat University, Bangkok, Thailand, e-mail: m.varalee@gmail.com

Authors' contribution:
A Study design · **B** Data collection · **C** Statistical analysis · **D** Data interpretation · **E** Manuscript preparation · **F** Literature search · **G** Funds collection

The CT scan is a useful diagnostic tool for staging and treatment planning in upper aerodigestive tract cancer (UATC) [1-3]. In routine conventional SECT, the protocol for UATC typically requires true non-contrast (TNC) imaging and post-contrast imaging in order to characterize tumour and lymph node enhancement.

This study aimed to qualitatively and quantitatively compare the attenuation values and the image quality of TNC and VNC datasets in patients with UATC, and to evaluate the potential radiation dose reduction by waiving the TNC phase.

Material and methods

Study population

The study was approved by the Human Ethics Committee of our institution. We retrospectively reviewed the medical records of patients with UATC at Thammasat University Hospital, Thailand, from January 2020 to November 2021.

The inclusion criteria were as follows: 1) patients who were 18 years old or above; 2) patients who had histopathologically confirmed UATC; 3) patients who underwent pre-treatment DLSCT. The exclusion criterion was patients who had severe imaging artifacts on CT scans.

Sixty-one consecutive patients were included in this study. Demographic data including age, sex, underlying disease, and an indication of the CT scan were collected from the medical records. The histopathological results were acquired from the pathological reports.

Imaging acquisition

All scans were performed using a dual-layer spectral CT scanner (Philips IQon Spectral CT and Spectral CT7500, Philips Healthcare, Eindhoven, Netherlands). All patients underwent a standard CT protocol of the institute, which included pre-contrast (true non-contrast, TNC) and post-contrast phases. Patients were placed in a supine position. All scans were performed with a 120 kVp tube voltage, 1.4:1 helical pitch, and 0.4-second rotation time with a reconstructed FOV of 512 mm^2. Automated mAS and beam collimation were applied and varied according to patient thickness. The detector configurations were 64 × 0.625 mm and 128 × 0.625 mm for Philips IQon Spectral CT and Spectral CT7500, respectively.

After an anteroposterior scout, TNC phase was scanned from skull base to aortic arch in the cranio-caudal direction. Subsequently, a weight adapted amount (1.5 mL/kg) of non-ionic iodinated contrast agent (Ultravist 300 MCT, Bayer Vital GmbH, Leverkusen, Germany) followed by a 30-mL saline chaser was injected intravenously with a rate of 2.5 mL/sec using a dual syringe injection system (Stellant, MEDRAD, Indianola, Pennsylvania). The post-contrast phase was acquired at 70 seconds after contrast administration in the same field of view and scan direction as performed on TNC. All datasets were reconstructed in the axial images by using a section thickness and an interval of 3.5 mm.

Imaging post-processing

The raw data were reconstructed using a specific spectral post-processing workstation (IntelliSpace Portal v.11, Philips Healthcare, Netherlands). The VNC images were obtained from post-contrast images using vendor-specific software (Figure 1). Axial TNC and VNC images were reconstructed using a section thickness and an interval of 3.5 mm.

Imaging assessment

For all CT images, quantitative analysis and qualitative assessment were retrospectively evaluated using a picture archiving and communications system (PACS) for CT attenuation value, imaging noise, and imaging quality. CT images were reviewed by 2 observers, a neuroradiologist with 10 years of experience and a third-year resident. Both observers were unaware of imaging acquisition. The location of each ROI and image quality of TNC and VNC images were obtained by consensus.

CT attenuation values of the tumour (Figure 2) and 4 other normal ipsilateral anatomic structures including the buccal fat pad, tonsillar region, sternocleidomastoid muscle, and medial pterygoid muscle were measured by placing regions of interests (ROIs) (Figure 3). Each of the ROIs was placed at the same imaging level and location in TNC and VNC images. VNC images were compared to TNC images regarding differences in CT attenuation values.

The standard deviations (SD) of the pixel value of subcutaneous fat at the anterior neck acquired from ROI placement was used to determine the imaging noise (Figure 4).

Therefore, a total of 6 ROIs (one tumour, 4 anatomic regions, and one noise subsite) were placed per TNC and VNC for individual subjects. The minimum area of individual ROI was at least 20 mm^2.

The subjective image quality was assessed by using a 5-point grade scale scoring system, which is the same method as in previous literature: 1 = not assessable due to severe artifacts or bad image quality; 2 = poor image quality from major artifacts; 3 = sufficient image quality that permits good confidence in image evaluation; 4 = good image quality with minor artifacts; 5 = excellent image quality without artifacts [4] (Figure 5). The level of acceptance for diagnosis purposes with VNC images was rated as 3. A score of 4 or more was considered as having the potential to replace TNC images.

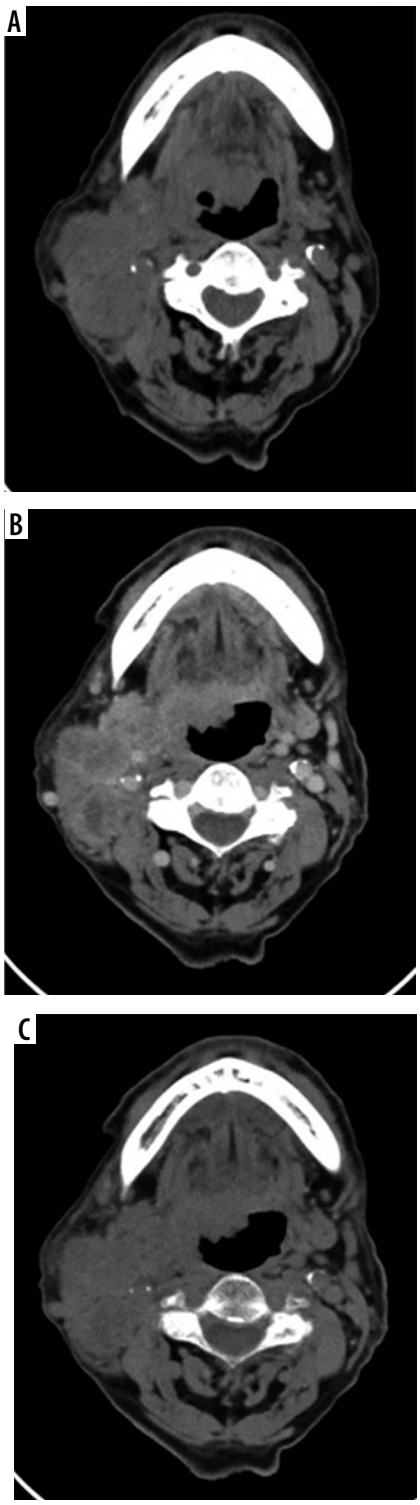

Figure 1. A 78-year-old woman with CA soft palate. **A**) Axial true non-contrast image was performed before intravenous contrast administration. **B**) Axial contrast-enhanced image was performed after intravenous contrast administration 70 seconds. **C**) Axial virtual non-contrast image was reconstructed due to iodine subtraction from the contrast-enhanced image by using postprocessing algorithms

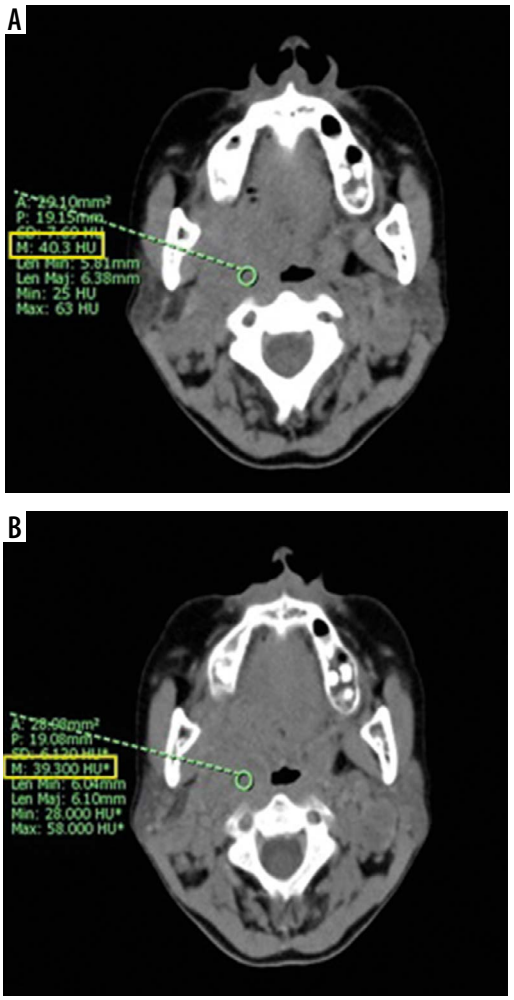

Figure 2. A 44-year-old woman with CA soft palate. Comparison of computed tomography attenuation values of the tumor at the same level between (**A**) axial true non-contrast image – 40.3 HU and (**B**) axial virtual non-contrast image – 39.3 HU

Radiation dose estimation

For each of the 2 phases, the dose-length product (DLP, mGy cm) was recorded from registered data using a CT scanner. The effective radiation doses (in millisieverts) for each phase were calculated by using the method proposed by the European Working Group for Guidelines on Quality criteria in CT, applying the following relationship: E = DLP × κ conversion coefficient. The neck κ conversion coefficient is 0.0054 mSv/mGy cm [5-7]. The effective dose of a biphasic TNC and post-contrast CT protocol was compared with a single-phase protocol (post-contrast CT with VNC reconstruction). The percentage of potential dose reduction by omitting TNC was calculated.

Statistical analysis

CT attenuation value, imaging noise, and quality on TNC and VNC images were interpreted in terms of the mean ± standard deviation. Mean differences in CT attenuation values, imaging noises, and quality between TNC

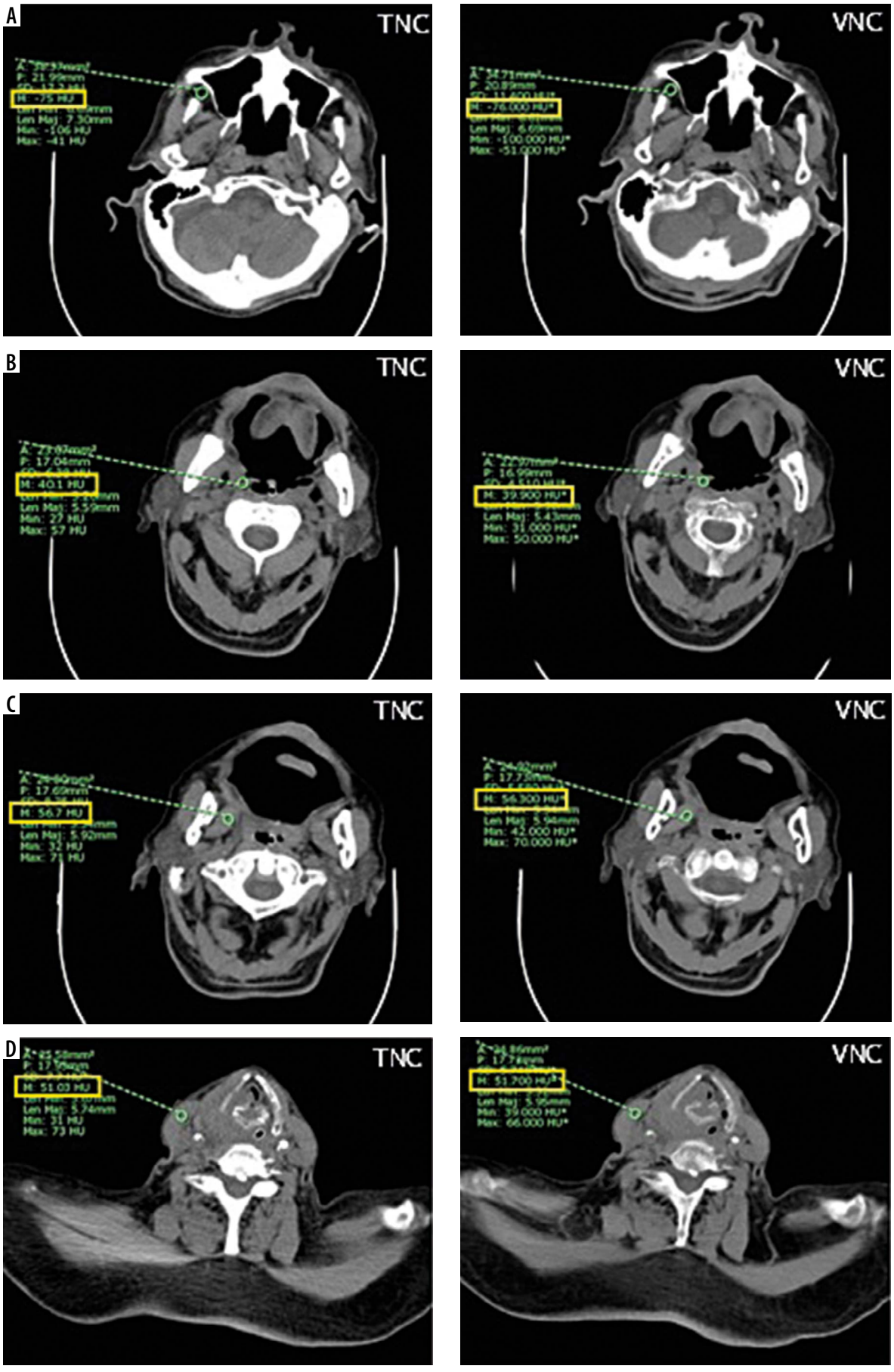

Figure 3. A 84-year-old man with CA supraglottic. Comparison of computed tomography attenuation values of the buccal fat pad (**A**), tonsillar region (**B**), medial pterygoid muscle (**C**), and sternocleidomastoid muscle (**D**) between axial true non-contrast images (upper row of figure) and axial virtual non-contrast images (lower row of figure) at the same level

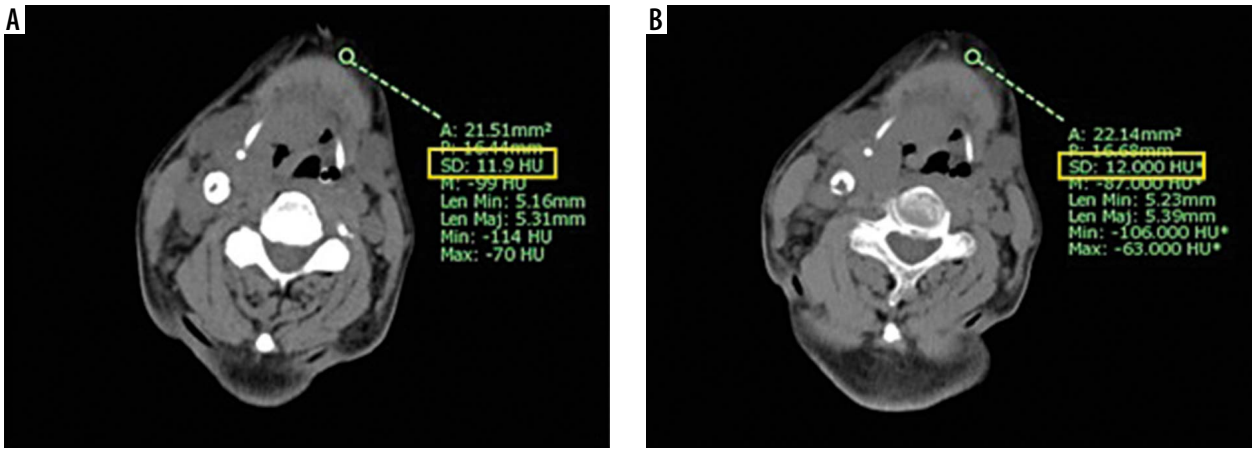

Figure 4: A 84-year-old man with CA supraglottic (the same patient as in Figure 3). To determine the imaging noise, the standard deviations (SD) of anterior subcutaneous fat of the neck were measured between (**A**) axial true non-contrast images – SD = 11.9 and (**B**) axial virtual non-contrast images – SD = 12.0 at the same level

and VNC images were compared using the paired *t*-test. Fisher's exact test was used for categorization of the image quality scores. The radiation dose of conventional biphasic TNC-post contrast protocol and a single post-contrast protocol with VNC reconstruction were analysed in terms of the mean ± standard deviation. Radiation dose reduction between the 2 protocols was expressed in percent ± standard deviation. All statistical analysis was performed by using statistical software software (R version 4.1.1, R Foundation for Statistical Computing, Vienna, Austria). A value of $p < 0.05$ indicated a statistically significant difference.

Results

Demographics

There were 61 consecutive patients included in this study; 47 patients were males and 14 patients were females. The mean age at diagnosis was 63.5±12.8 years (age range 35-91 years). All patients had histopathological results of upper aerodigestive tract cancer in various locations (nasal cavity and paranasal sinuses, $n = 4$; nasopharynx, $n = 5$; oropharynx, $n = 8$; hypopharynx, $n = 7$; oral cavity, $n = 17$; larynx, $n = 20$). Details of patients' demographic data are summarized in Table 1.

CT attenuation values

There was no statistical difference in the mean CT attenuation values between TNC and VNC images for tumour and all tissue types, except for the buccal fat pad. The mean CT attenuation values of all tissue types were as follows: tumour; 43.6 ± 6.5 HU on TNC and 44.0 ± 6.8 HU on VNC ($p = 0.3969$), buccal fat pad; –89.2 ± 14.6 HU on TNC and –88.5 ± 14.5 HU on VNC ($p = 0.0074$), tonsillar region; 45.9 ± 6.3 HU on TNC and 46.2 ± 5.4 HU on VNC ($p = 0.4401$), medial pterygoid muscle; 60.4 ± 5.8 HU on TNC and 60.1 ± 5.8 HU on VNC ($p = 0.0919$), and sternocleidomastoid muscle; 55.2 ± 6.1 HU on TNC and 54.7 ± 6.0 HU on VNC ($p = 0.3593$). The greatest differences between TNC and VNC images were detected in buccal fat pad (–0.7 ± 2.0). Mean CT attenuation values and *p*-values are presented in Table 2.

In all tissue types, the difference in mean CT attenuation values between TNC and VNC images was less than 15 HU (Figure 6).

Overall, 97% of all scans had a difference in mean CT attenuation values less than 10 HU. The difference of mean CT attenuation values between TNC and VNC images was less than 10 HU in 96.7%, 98.4%, 98.4%, and 91.8% of the tumour, buccal fat pad, tonsillar region, and sternocleidomastoid muscle, respectively. There was no difference in mean CT attenuation values greater than 10 HU of medial pterygoid muscle between TNC and VNC images. The frequency of cases with absolute differences in mean CT attenuation less than 10 HU is shown in Figure 7.

Imaging noise

The mean SD for imaging noise was 8.8 ± 2.5 and 8.7 ± 2.5 in TNC and VNC, respectively. There was no significant difference in imaging noise between TNC and VNC ($p = 0.5455$) (Table 2).

In total, there were 732 ROIs acquired from 5 different tissues and one noise from 61 patients in 2 datasets (TNC and VNC).

Image quality

By using a 5-point grading system, the image quality was rated as excellent quality (score 5) in 47 (77%) and 49 (80.3%) of TNC and VNC studies, respectively. There

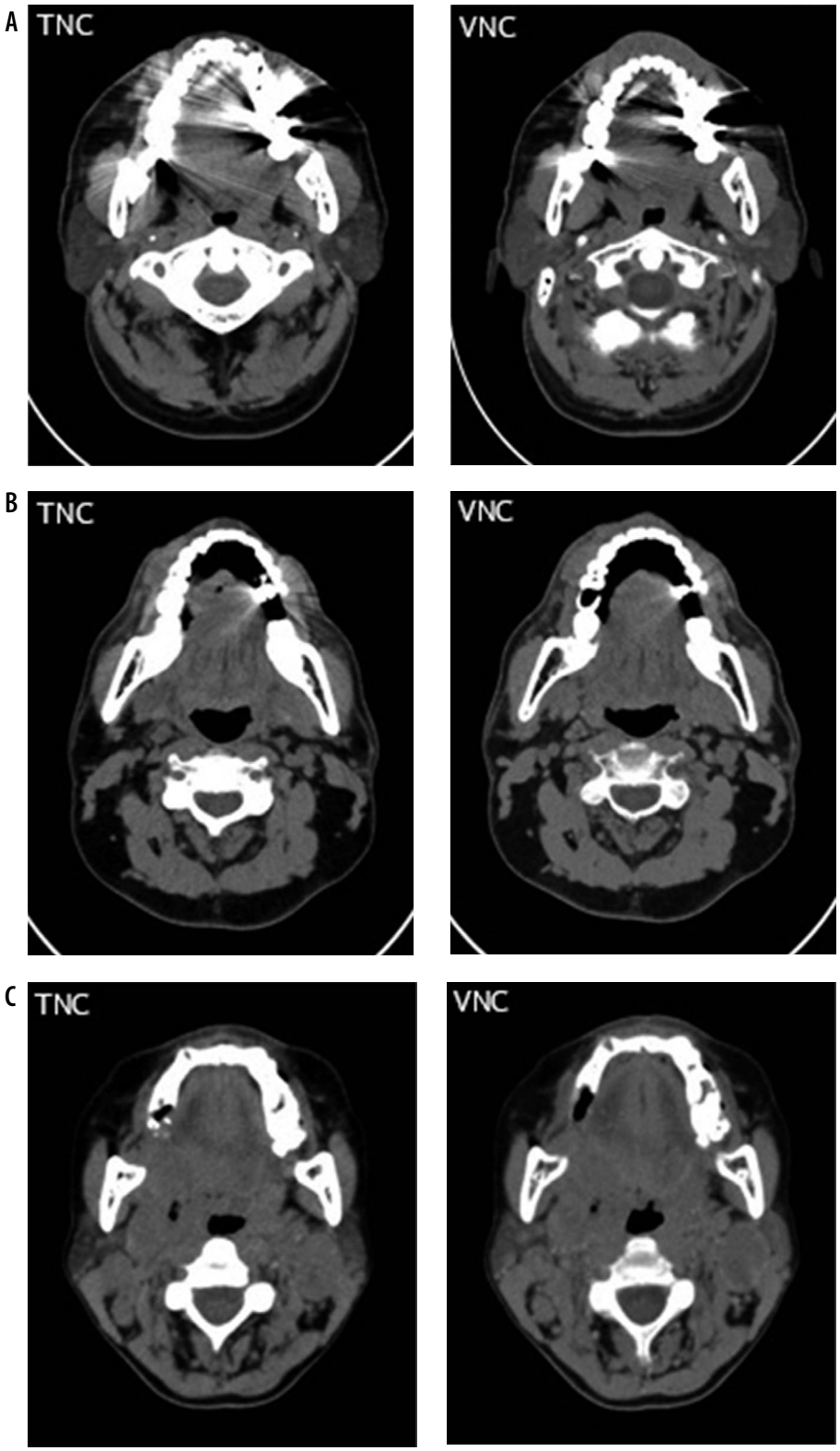

Figure 5: Image quality evaluation in different patients between axial TNC images (upper row of figure) and axial VNC images (lower row of figure) at the same level. **A**) IQ score=3; sufficient image quality with moderate artifacts in both images, (**B**) IQ score=4; good image quality with minor artifacts in both images, (**C**) IQ score=5; excellent image quality without artifacts in both images

Table 1. Patient demographics ($N = 61$)

Factor	
Age, years	
Mean (SD)	63.5 (12.8)
Range	35-91
Gender, *n* (%)	
Male	47 (77)
Female	14 (23)
Location, *n* (%)	
Nasal cavity and paranasal sinuses	4 (6.6)
Nasopharynx	5 (8.2)
Oropharynx	8 (13.1)
Hypopharynx	7 (11.5)
Oral cavity	17 (27.9)
Larynx	20 (32.8)
Histopathological result, *n* (%)	
Squamous cell carcinoma	59 (96.72)
Adenoid cystic carcinoma	1 (1.64)
Neuroendocrine carcinoma	1 (1.64)

Table 3. Image quality between true non-contrast and virtual non-contrast images

Image quality	TNC *n* (%)	VNC *n* (%)	*p*-value
1 (not assessable)	0	0	0.159
2 (poor)	0	0	
3 (sufficient)	10 (16.4)	10 (16.4)	
4 (good)	4 (6.6)	2 (3.3)	
5 (excellent)	47 (77.0)	49 (80.3)	
Mean (SD)	4.61 (0.76)	4.64 (0.75)	

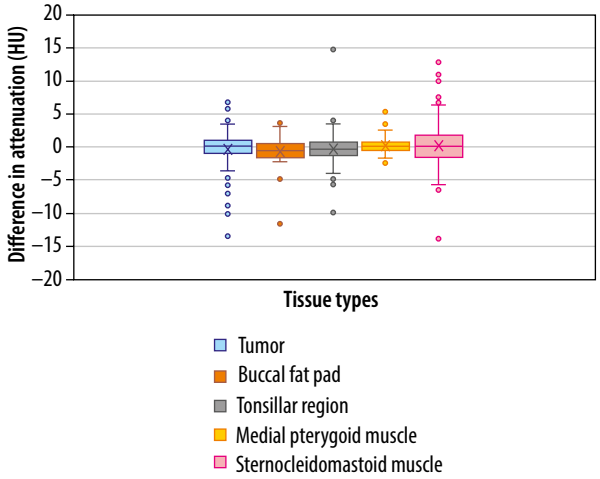

Figure 6. Box-and-whisker plots of the differences in HU between the true non-contrast and virtual non-contrast images. The box indicates the 25th and 75th quartile; the horizontal line indicates the median and the cross indicates the mean. Whiskers show the 5th and 95th percentiles; outliers are performed by the circles

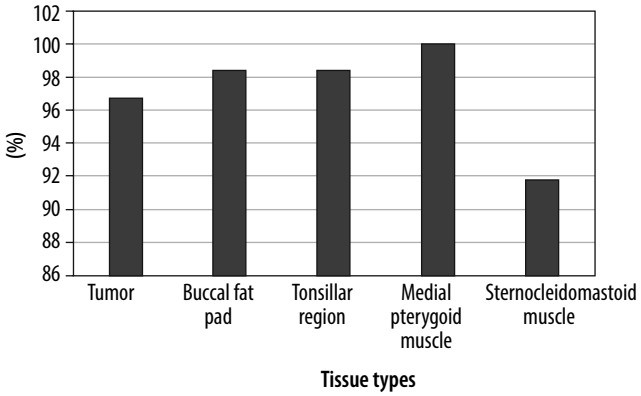

Figure 7. Differences in computed tomography attenuation values < 10 HU between the true non-contrast and virtual non-contrast images

Table 2. Mean computed tomography attenuation values, imaging noise, and *p*-values between true non-contrast and virtual non-contrast images

CT attenuation value (HU)	TNC Mean (SD)	VNC Mean (SD)	Difference Mean (SD)	Difference > 10 HU *n* (%)	*p*-value
Tumour	43.6 (6.5)	44 (6.8)	–0.4 (3.3)	2 (3.3)	0.3969
Buccal fat pad	–89.2 (14.6)	–88.5 (14.5)	–0.7 (2)	1 (1.6)	0.0073
Tonsillar region	45.9 (6.3)	46.2 (5.4)	–0.3 (3.1)	1 (1.6)	0.4401
Medial pterygoid muscle	60.4 (5.8)	60.1 (5.8)	0.3 (1.3)	0 (0)	0.0919
Sternocleidomastoid muscle	55.2 (6.1)	54.7 (6)	0.5 (4.3)	5 (8.2)	0.3593
Noise	8.8 (2.5)	8.7 (2.5)	0.1 (1.4)	0 (0)	0.5455

*Statistically significant at *p*-value < 0.05 determined by the paired *t*-test

Table 4. Effective radiation dose in 2-phase protocol and dose reduction by omitting the conventional unenhanced computed tomography scan

	Pre-contrast phase	Post-contrast phase	Pre- and post-contrast phases	Radiation dose reduction (%)
DLP (mGy-cm)				
Mean (SD)	474.7 (307.9)	486.2 (327.7)	960.9 (631.6)	49.5 (3.5)
ED (mSv)				
Mean (SD)	2.6 (1.7)	2.6 (1.8)	5.2 (3.4)	49.5 (3.5)

were 4 (6.6%) TNC studies and 2 (3.3%) VNC studies assessed as good quality (score 4). Both TNC and VNC were rated as sufficient quality (score 3) in 10 (16.4%) and 10 (16.4%) of the TNC and VNC studies, respectively. None of the studies was rated below the score of 3. Image quality of TNC and VNC images had average scores of 4.61 ± 0.76 and 4.64 ± 0.75, respectively. There was no significant difference of image quality between TNC and VNC ($p = 0.159$) (Table 3).

Radiation dose

The mean effective radiation doses for the TNC and post-contrast scan were 2.6 ± 1.7 mSv and 2.6 ± 1.8 mSv, respectively. For the combined biphasic TNC and post-contrast CT protocol, the total mean effective dose was 5.2 ± 3.4 mSv. To summarize, the percentage of potential dose reduction by omitting the conventional unenhanced CT scan was 49.5 ± 3.5% (Table 4).

Discussion

VNC imaging is one of the promising capabilities of DECT that can provide imaging theoretically resembling TNC images from an iodine elimination technique, which is performed on a material decomposition basis [8-13]. DLSCT is a novel technique of DECT, generating imaging from a specialized layered CT detector [2,7, 14-18]. One of the major advantages of DLSCT over other techniques of DECT – dual-source DECT and rapid kilovolt peak (kVp) switching DECT – is that DLSCT is always on dual-energy mode with availability of retrospective analysis for every scan. Thus, there is no need for pre-planning and pre-selection of the dual-energy mode in DSLCT [13,15,19].

CT scan of the neck is an essential imaging modality for UATC in pre-treatment staging and treatment planning. Routine protocol of CT neck in UATC typically requires a biphasic TNC and post-contrast CT protocol aiming to characterize the enhancing pattern of the tumour. A single-phase protocol (post-contrast CT with VNC reconstruction) available from DSLCT has advantages over conventional biphasic TNC protocol owing to decreased examination time and radiation dose [2,20].

There have been several previous studies that mainly researched the clinical feasibility of using VNC images in abdominal imaging from various DECT systems, including detecting aortic endoleak after endovascular repair, urinary or biliary stones, intracranial bleeding, mediastinal lymph nodes, and characterizing masses such as renal, solitary pulmonary nodule, hepatic, pancreas, and gastric masses [21-30]. Most of them revealed that VNC images were useful and feasible. Sauter *et al.* studied VNC acquired from DLSCT in abdominal imaging and found that VNC imaging is a promising tool for clinical usage with radiation dose reduction and enhanced diagnostic value of a single-phase post-contrast CT [23]. Similar results were reported by Mileto *et al.*, who worked on VNC generated from dual-source DECT in pancreatic imaging [27]. They found that VNC had no significant difference in image quality but lower imaging noise and radiation dose compared to TNC. Shi *et al.* also concluded that VNC can potentially replace TNC in evaluation of gastric tumours by using dual-source DECT [25]. Meyer *et al.* also reported strong correlation between VNC and TNC for characterization of renal lesions. However, VNC had lower diagnostic performance for depicting contrast-enhanced versus non-enhanced renal lesions as compared to TNC [24].

On the other hand, a few studies reported different results. Durieux *et al.* concluded that VNC images created from third-generation dual-source DECT still should not replace TNC images because of substantial differences in attenuation measurements [21]. Similar results were also reported by Lehti *et al.*, who studied VNC based on arterial phase CT angiography acquired from dual-source DECT. They found that VNC had a significantly different mean attenuation value and higher imaging noise as compared to TNC [22].

There were limited publications regarding VNC images in head and neck imaging. Beland *et al.* found that VNC acquired from rapid kilovolt peak (kVp) switching DECT could eliminate TNC in the diagnosis of sialolithiasis in the major salivary gland [31]. Studies by Fu *et al.* on VNC imaging for several diseases of cervical lymph nodes concluded that VNC in conjunction with post-contrast imaging provided clear images in the diagnosis of enlarged cervical lymph nodes [32]. However, they did not mention the DECT system used in the study.

To our knowledge, there has been no previous comparative study between VNC and TNC generated from DLSCT in patients with UATC.

CT attenuation values, imaging noise, and imaging quality are the key issues regarding potential replacement of TNC by VNC images [4,20-30,32,33].

This study showed no statistical difference in the mean CT attenuation values between TNC and VNC images for UATC and other tissues (tonsillar region, medial pterygoid muscle, and sternocleidomastoid muscle), except for buccal fat pad ($p = 0.007$). The significant difference in the CT attenuation value of buccal fat was due to the high variability of attenuation from the ROI measurement on both TNC and VNC for unknown reasons. For buccal fat pad, VNC images had a slightly higher mean CT attenuation value (–88.5 ± 14.5) than for TNC (–89.2 ± 14.6). However, there was only one study that showed a difference in mean CT attenuation value greater than 10 HU for buccal fat. Similar results were described by Sauter *et al.,* who found a difference in abdominal fat CT value between TNC and VNC [23]. Because fat is a tissue with relatively little contrast enhancement, there should be a minimal amount of iodine to be subtracted, so the exact explanation for this difference between TNC and VNC images is still unsolved [23].

According to the results of previous studies, VNC images in which the difference in CT attenuation values was lower than 15 HU were considered relevant in most clinical situations [23]. Our results showed no difference of CT attenuation values greater than 15 HU in all tissue types. Furthermore, 97% of all images had a difference of less than 10 HU between TNC and VNC images. Therefore, VNC images of the neck have potential value for clinical usage.

We used image noise as a representative parameter for the quantitative image quality [34]. Our results showed no statistical difference between TNC and VNC images regarding imaging noise. However, VNC images had slightly lower mean imaging noise than TNC images. This is due to the rendering algorithm in the post-processing technique, creating a smoother image [20,25,34].

In our experience, there was no significant difference in subjective image quality between TNC and VNC images. VNC images had slightly higher average scores of image quality than TNC images. All VNC images were rated as score 3 or more, which is acceptable quality for diagnostic purposes. The VNC images were good quality and were nearly equivalent to TNC images.

The possibility of removing TNC has the benefits of reduced examination time and decreased risk of radiation-induced malignancies, particularly thyroid cancer, because the thyroid is a radiosensitive organ [3,27]. This study demonstrated 49.5 ± 3.5% reduction of radiation dose by omitting TNC.

The present study had some limitations. First, we presented a qualitative and quantitative comparison of TNC and VNC datasets but did not show the accuracy for tumour staging in UATC. However, we assumed that the accuracy for tumour staging on VNC images should be similar on TNC images because there was no significant difference in CT attenuation values between these acquisitions. Second, CT attenuation values in the metastatic cervical nodes could not be evaluated because the accurate discrimination between benign and metastasis by histopathological result for individual lymph nodes was unavailable in this retrospective study. Third, we did not study CT attenuation of the thyroid gland, which has natural intrinsic iodine content and might have different iodine subtraction results from other structures. These should be interesting issues to inspect in the future. Finally, this study was performed using only DSLCT while other DECT systems were unavailable for comparison. Because various DECT systems are limited in most institutions, further multi-centre studies would be challenging.

Conclusions

In our experience, the VNC images were obtained from postprocessing algorithms of the DSLCT. These results confirmed that VNC images provide qualitative and quantitative datasets of good image quality, similar to TNC images. Thus, VNC images are a feasible alternative for implementation in patients with UATC, with the advantage of radiation dose reduction by waiving the TNC phase.

Conflicts of interest

The authors report no conflict of interest.

References

1. Forghani R, Kelly HR, Curtin HD. Applications of dual-energy computed tomography for the evaluation of head and neck squamous cell carcinoma. Neuroimaging Clin N Am 2017; 27: 445-459.
2. Roele ED, Timmer VC, Vaassen LA, et al. Dual-energy CT in head and neck imaging. Curr Radiol Rep 2017; 5: 19. doi: 10.1007/s40134-017-0213-0.
3. Vogl TJ, Schulz B, Bauer RW, et al. Dual-energy CT applications in head and neck imaging. Am J Roentgenol 2012; 199: S34-S39.
4. De Cecco CN, Muscogiuri G, Schoepf UJ, et al. Virtual unenhanced imaging of the liver with third-generation dual-source dual-energy CT and advanced modeled iterative reconstruction. Eur J Radiol 2016; 85: 1257-1264.

5. Gerber TC, Kuzo RS, Morin RL. Techniques and parameters for estimating radiation exposure and dose in cardiac computed tomography. Int J Cardiovasc Imaging 2005; 21: 165-176.
6. Menzel H, Schibilla H, Teunen D. European guidelines on quality criteria for computed tomography. Luxembourg: European Commission; 2000, 16262.
7. Hamid S, Nasir MU, So A, et al. Clinical applications of dual-energy CT. Korean J Radiol 2021; 22: 970-982.
8. Forghani R. An update on advanced dual-energy CT for head and neck cancer imaging. Expert Rev Anticancer Ther 2019; 19: 633-644.
9. Forghani R, Mukherji S. Advanced dual-energy CT applications for the evaluation of the soft tissues of the neck. Clin Radiol 2018; 73: 70-80.
10. Albrecht MH, Vogl TJ, Martin SS, et al. Review of clinical applications for virtual monoenergetic dual-energy CT. Radiology 2019; 293: 260-271.
11. Nair JR, Burrows C, Jerome S, et al. Dual energy CT: a step ahead in brain and spine imaging. Br J Radiol 2020; 93: 20190872. doi: 10.1259/bjr.20190872.
12. Patino M, Prochowski A, Agrawal MD, et al. Material separation using dual-energy CT: current and emerging applications. Radiographics 2016; 36: 1087-1105.
13. Marin D, Boll DT, Mileto A, Nelson RC. State of the art: dual-energy CT of the abdomen. Radiology 2014; 271: 327-342.
14. Sananmuang T, Agarwal M, Maleki F, et al. Dual energy computed tomography in head and neck imaging: pushing the envelope. Neuroimaging Clin N Am 2020; 30: 311-323.
15. Forghani R, De Man B, Gupta R. Dual-energy computed tomography: physical principles, approaches to scanning, usage, and implementation: Part 2. Neuroimaging Clin N Am 2017; 27: 385-400.
16. Forghani R, De Man B, Gupta R. Dual-energy computed tomography: physical principles, approaches to scanning, usage, and implementation: Part 1. Neuroimaging Clin N Am 2017; 27: 371-384.
17. Forghani R, Kelly H, Yu E, et al. Low-energy virtual monochromatic dual-energy computed tomography images for the evaluation of head and neck squamous cell carcinoma: a study of tumor visibility compared with single-energy computed tomography and user acceptance. J Comput Assist Tomogr 2017; 41: 565-571.
18. Forghani R, Srinivasan A, Forghani B. Advanced tissue characterization and texture analysis using dual-energy computed tomography: horizons and emerging applications. Neuroimaging Clin N Am 2017; 27: 533-546.
19. Simsir BD, Danse E, Coche E. Benefit of dual-layer spectral ct in emergency imaging of different organ systems. Clin Radiol 2020; 75: 886-902.
20. Graser A, Johnson TR, Hecht EM, et al. Dual-energy ct in patients suspected of having renal masses: Can virtual nonenhanced images replace true nonenhanced images? Radiology 2009; 252: 433-440.
21. Durieux P, Gevenois PA, Muylem AV, et al. Abdominal attenuation values on virtual and true unenhanced images obtained with third-generation dual-source dual-energy ct. Am J Roentgenol 2018; 210: 1042-1058.
22. Lehti L, Söderberg M, Höglund P, et al. Reliability of virtual non-contrast computed tomography angiography: comparing it with the real deal. Acta Radiol Open 2018; 7: 2058460118790115. doi: 10.1177/2058460118790115
23. Sauter AP, Muenzel D, Dangelmaier J, et al. Dual-layer spectral computed tomography: virtual non-contrast in comparison to true non-contrast images. Eur J Radiol 2018; 104: 108-114.
24. Meyer M, Nelson RC, Vernuccio F, et al. Virtual unenhanced images at dual-energy CT: influence on renal lesion characterization. Radiology 2019; 291: 381-390.
25. Shi L, Yan F, Pan Z, et al. Stomach virtual non-enhanced ct with second-generation, dual-energy CT: a preliminary study. PLoS One 2014; 9: e112295.
26. Yoo SY, Kim Y, Cho HH, et al. Dual-energy CT in the assessment of mediastinal lymph nodes: Comparative study of virtual non-contrast and true non-contrast images. Korean J Radiol 2013; 14: 532-539.
27. Mileto A, Mazziotti S, Gaeta M, et al. Pancreatic dual-source dual-energy CT: is it time to discard unenhanced imaging? Clin Radiol 2012; 67: 334-339.
28. De Cecco CN, Buffa V, Fedeli S, et al. Dual energy CT (DECT) of the liver: conventional versus virtual unenhanced images. Eur Radiol 2010; 20: 2870-2875.
29. Jiang X, Zhang S, Xie Q, et al. Evaluation of virtual noncontrast images obtained from dual-energy cta for diagnosing subarachnoid hemorrhage. Am J Neuroradiol 2015; 36: 855-860.
30. Cho SB, Baek HJ, Ryu KH, et al. Initial clinical experience with dual-layer detector spectral ct in patients with acute intracerebral haemorrhage: a single-centre pilot study. PLoS One 2017; 12: e0186024. doi: 10.1371/journal.pone.0186024.
31. Beland B, Levental M, Srinivasan A, Forghani R. Practice variations in salivary gland imaging and utility of virtual unenhanced dual energy CT images for the detection of major salivary gland stones. Acta Radiol 2019; 60: 1144-1152.
32. Fu F, He A, Zhang Y, et al. Dua-energy virtual noncontrast imaging in diagnosis of cervical metastasis lymph nodes. J Cancer Res Ther 2015; 11 Suppl 2: C202-C204.
33. Kawamoto S, Zhou XR, Leidecker C, et al. Virtual noncontrast renal imaging using dual-energy CT: evaluation of CT numbers of renal parenchyma and renal masses. Imaging in Medicine 2011; 3: 501-511.
34. Nakayama Y, Awai K, Funama Y, et al. Abdominal CT with low tube voltage: preliminary observations about radiation dose, contrast enhancement, image quality, and noise. Radiology 2005; 237: 945-951.